

Fine Timing and Frequency Synchronization for MIMO-OFDM: An Extreme Learning Approach

Jun Liu, Kai Mei, Xiaochen Zhang, Des McLernon, *Member, IEEE*, Dongtang Ma, *Senior Member, IEEE*, Jibo Wei, *Member, IEEE* and Syed Ali Raza Zaidi, *Senior Member, IEEE*

Abstract—Multiple-input multiple-output orthogonal frequency-division multiplexing (MIMO-OFDM) is a key technology component in the evolution towards cognitive radio (CR) in next-generation communication in which the accuracy of timing and frequency synchronization significantly impacts the overall system performance. In this paper, we propose a novel scheme leveraging extreme learning machine (ELM) to achieve high-precision synchronization. Specifically, exploiting the preamble signals with synchronization offsets, two ELMs are incorporated into a traditional MIMO-OFDM system to estimate both the residual symbol timing offset (RSTO) and the residual carrier frequency offset (RCFO). The simulation results show that the performance of the proposed ELM-based synchronization scheme is superior to the traditional method under both additive white Gaussian noise (AWGN) and frequency selective fading channels. Furthermore, comparing with the existing machine learning based techniques, the proposed method shows outstanding performance without the requirement of perfect channel state information (CSI) and prohibitive computational complexity. Finally, the proposed method is robust in terms of the choice of channel parameters (e.g., number of paths) and also in terms of “generalization ability” from a machine learning standpoint.

Index Terms—Extreme learning machine, timing, frequency synchronization, MIMO-OFDM, frequency selective fading.

I. INTRODUCTION

COGNITIVE radio (CR) in fifth generation (5G) cellular communications technology for commercial use is currently being deployed in various countries. Meanwhile, research into sixth generation (6G) systems is already under way as it is designed to meet the needs of ultra-high capacity, reliability and low latency [1]. Among existing and future technologies, the key enabling technologies CR and multiple-input multiple-output orthogonal frequency-division multiplexing (MIMO-OFDM) will continue to play important roles that facilitate development and deployment. To improve spectral efficiency, CR enables nodes to explore and use underutilized licensed channels. And meanwhile, as an effective physical layer solution, the spectral efficiency (SE) of OFDM systems is superior to conventional single carrier systems and it can

combat inter-symbol interference (ISI) through transforming a frequency-selective fading channel into many parallel flat-fading subchannels.

However, OFDM systems are highly sensitive to carrier frequency offset (CFO) which can destroy the important orthogonality between subcarriers and this results in the degradation of bit error rate (BER) performance. Therefore, the estimation of accurate CFO is crucial to OFDM systems. Meanwhile, symbol timing offset (STO) can result in ISI and a rotated phase whose value is proportional to the subcarrier index at the FFT output in an OFDM receiver. These issues severely degrade the efficiency of CR and the performance of communications systems [2].

The traditional approach towards the estimation of both STO (also known as the timing synchronization) and CFO (also known as the frequency synchronization), involves sending a preamble at OFDM transmitters and processing the signals at the receivers. These signal processing techniques have been studied extensively, and many seminal articles have been published since the 1990s. P.H. Moose addressed the issue of receiver frequency synchronization by proposing an algorithm for a maximum likelihood estimate (MLE) of the CFO using the discrete Fourier transform (DFT) of a repeated symbol, and a lower bound for signal-to-noise (SNR) has been derived [3]. In [4], a method for the rapid and robust frequency and timing synchronization for OFDM has been presented by Schmidl *et al.* Then, an implementation of an MIMO-OFDM-based wireless local area network (WLAN) system was demonstrated by [5], in which a simple MIMO extension of Schmidl’s algorithm [4] proposed in [6] was deployed in a practical system. In [7] the authors address the problem of training design for a frequency-selective channel and also CFO estimation in single- and multiple-antenna systems under different energy-distribution constraints. In [8] and [9], a new framework referred to as sparse blind CFO estimation for interleaved uplink orthogonal frequency-division multiple access (OFDMA) and the sparse recovery assisted CFO estimator for the uplink OFDMA were respectively proposed. Timing and frequency synchronization, as well as channel estimation can be carried out jointly to achieve better performance. [10] presents a novel preamble-aided method for joint estimation of timing, CFO, and channel parameters for OFDM. [11] considered the joint maximum likelihood estimator for the channel impulse response (CIR) and the CFO. In [12], a comprehensive literature review and classification of the recent research progress in timing and carrier synchronization was presented.

This work was supported in part by the China Scholarship Council (CSC), National Natural Science Foundation of China (NSFC) under Grant 61931020, 61372099 and 61601480. (*Corresponding author: Dongtang Ma and Jun Liu.*)

Jun Liu, Kai Mei, Xiaochen Zhang, Dongtang Ma, and Jibo Wei are with the College of Electronic Science and Technology, National University of Defense Technology, Changsha 410073, China (E-mail: {liujun15, meikai11, zhangxiaochen14, dongtangma, wjbhw}@nudt.edu.cn).

Des McLernon, Jun Liu and Syed Ali Raza Zaidi are with the School of Electronic and Electrical Engineering, University of Leeds, Leeds, LS2 9JT, UK (E-mail: {D.C.McLernon, eljliu, S.A.Zaidi}@leeds.ac.uk).

But, errors will nearly always remain in the estimation of STO and CFO, which are also known as residual STO (RSTO) and residual CFO (RCFO). This is due to the effects of fading and thermal noise. The influence of STO errors on channel interpolation is analyzed in [13]. Even a small RCFO can result in amplitude and phase distortion and also inter-carrier interference (ICI) among subcarriers. Traditionally, in order to mitigate the impact of RCFO, channel tracking methods are employed, and this is realized by inserting known pilots into specific subcarriers. However, this method reduces system SE. As regards RSTO, a compensation method for channel correction needs to be used. To reduce the sensitivity to synchronization errors, [14] develops conditions for the selection of appropriate Zadoff-Chu sequences and then designs a training sequence and proposes joint signal detection, timing, and CFO estimation algorithms for OFDM downlink transmissions.

In recent years, challenges to traditional methods have emerged that use data-based approaches relying on machine learning [15]–[19]. A popular scheme is machine learning-based end-to-end communications systems. Based on the idea of autoencoder, Dörner *et al.* proposes a learning-based communications system, in which the task of synchronization is addressed through a neural network [20]. Similarly, in [21], a sampling time synchronization model using a convolutional neural network (CNN) for end-to-end communications systems is introduced. In [22], an extreme learning machine (ELM)-based frame synchronization method for a burst-mode communications system is proposed. The work in [23] uses CNN to achieve adaptive modulation and coding in MIMO-OFDM systems with practical impairments, such as imperfect synchronization and channel estimation. Finally, [24] investigates a deep neural network (DNN)-based solution for packet detection and CFO estimation.

Although the above-mentioned machine learning-based schemes achieve better performance or robustness than traditional methods, their shortcomings lead to serious difficulties in practical implementation. We summarize the challenges and deficiencies of these schemes as follows.

- In previous machine learning related works [15]–[20], the synchronization aspects are ignored and perfect synchronization is assumed. Since the trained parameters of the neural network depend significantly on the input data, when the test signal has STO and CFO, these methods would crash.
- The mathematical theory of communication was exhaustively explored by Shannon in [25], where the fundamental problem is described as “reproducing at one point either exactly or approximately a message selected at another point”. But, autoencoder-based methods [20], [21] present a “chicken and egg” problem. That is to say, you first need a reliable communications system to do the error back-propagation to actually train an end-to-end communications system for you. Therein lies the paradox.
- The schemes in [21]–[24] sink into another kind of “chicken and egg” dilemma. Specifically, in the training stage, they require the accurate probability density

function (PDF) of a channel to generate labeled data with exact timing location and CFO. Unfortunately, it is impossible to priorly acquire the PDF of a fading channel in real scenarios. Besides, to train these schemes under a real channel, the target output, exact timing location and CFO are impossible to acquire.

- The common disadvantage of most of the current learning-based techniques lies in the computational complexity because they are based on a DNN. DNNs usually have deep hidden layers, which requires prohibitive computational complexity.

Motivated by the challenges mentioned above, in this paper we first propose a robust ELM-based fine timing and frequency synchronization scheme to deal with the challenges above. Unlike previous learning schemes, where a reliable feedback link between the transmitter and receiver or an accurate channel PDF is necessary, we deploy an ELM at the receiver and we generate training data by letting the preamble be corrupted by RSTO and RCFO without the effects of multipath fading channel and thermal noise. There are two main reasons for this. The first aims to make ELM learn the relationship between the corrupted preamble and its corresponding RSTO and RCFO. The second reason is to avoid the need for the channel PDF. Specifically, we combine ELMs to a typical MIMO-OFDM system instead of using an end-to-end autoencoder-based model so that the training can be carried out entirely at the receiver. Then, the estimation of both STO and CFO rely on that the preamble signal is perfectly known for the receiver and it consists two identical parts. Therefore, we let the ELMs to learn the sequences of the original preamble and the corrupted preambles with RSTO and RCFO instead of sequences of the preambles corrupted by a fading channel with a given PDF. These two strategies prevent our proposed schemes sink into the “chicken and egg” dilemma. In addition, an ELM only has one hidden layer so its computational complexity of training and prediction is significantly lower than a DNN. The main contributions of this paper are summarized as follows.

- For MIMO-OFDM, we incorporate ELM with a traditional STO estimator. In the proposed scheme, coarse synchronization is carried out by using autocorrelation-based algorithm. Then, the fine timing synchronization can be achieved by ELM without the need for any prior information about the channel.
- We first propose a robust ELM-based scheme to realize RCFO estimation without the need for additional prior information about the channel, where the ELM can learn the mapping relationship between the preamble corrupted by both RSTO and RCFO.
- We give the comparison of the complexity between the proposed ELM-based models and the traditional algorithm and DNN-based methods. Then, the performance analysis of the proposed learning scheme in different cases is provided. Specifically, computer simulation results show that the proposed scheme is superior to traditional STO and CFO estimation methods in terms of mean squared error (MSE). In addition, extensive simulation results and comparisons have demonstrated the

robustness and (machine learning) generalization ability of the proposed scheme.

The remainder of this paper is organized as follows. The signal model of the MIMO-OFDM system and traditional timing and frequency synchronization for MIMO-OFDM are presented in Sections II and III, respectively. In Section IV, we propose a scheme that incorporates ELM into the traditional MIMO-OFDM system, in which ELM is used to estimate RSTO and RCFO. Then, numerical results and analysis for evaluating the performance of the proposed scheme are provided in Section V, which is followed by conclusions in Section VI.

Notations: The notations adopted in the paper are as follows. We use boldface lowercase \mathbf{x} and capital letters \mathbf{X} to denote column vectors and matrices, respectively. Superscripts $^{-1}$, $*$, T , H and † stand for inverse, conjugate, transpose, Hermitian transpose and Moore-Penrose pseudoinverse, respectively. In addition, \otimes , \odot , \oslash , $E\{\cdot\}$, $\lfloor \cdot \rfloor$ and $j = \sqrt{-1}$ denote respectively the Kronecker product, Hadamard product, cyclic convolution, the expectation operation, floor function and the imaginary unit. Note that $\angle(\cdot)$ returns the phase angle of a complex number. Finally, $\text{repmat}(\mathbf{A}, m, n)$ returns an array containing m and n copies of \mathbf{A} in the column and row dimensions, respectively.

II. MIMO-OFDM SIGNAL MODEL

Let us now consider a MIMO-OFDM system with N_t transmit (TX) and N_r receive (RX) antennas, which is usually denoted as a $N_t \times N_r$ system. Without loss of generality, we consider the frequency-domain MIMO-OFDM signal model, which is directly given as [5]

$$\tilde{\mathbf{x}}(a) = \tilde{\mathbf{H}}\tilde{\mathbf{s}}(a) + \tilde{\mathbf{n}}(a) \quad (1)$$

where an $N_r N_c$ -dimensional complex vector $\tilde{\mathbf{x}}(a)$ represents the frequency-domain received signal, $\tilde{\mathbf{s}}(a) = [\mathbf{s}(0, a)^T, \dots, \mathbf{s}(N_c - 1, a)^T]^T \in N_t N_c \times 1$ and $\mathbf{s}(k, a)$ represents an N_t -dimensional complex vector transmitted on the k th subcarrier of the a th MIMO-OFDM symbol with $S_p(k, a)$ as its p th element, i.e., transmitted on the p th TX antenna. $\tilde{\mathbf{n}}(a)$ represents the frequency-domain noise vector, with i.i.d. zero-mean, complex Gaussian elements with variance $0.5\sigma_n^2$ per dimension, and the channel frequency response is represented as a block diagonal matrix $\tilde{\mathbf{H}}$ as follows:

$$\tilde{\mathbf{H}} = \begin{bmatrix} \mathbf{H}(0) & & 0 \\ & \ddots & \\ 0 & & \mathbf{H}(N_c - 1) \end{bmatrix}. \quad (2)$$

Now, $\mathbf{H}(k) \in \mathbb{C}^{N_r \times N_t}$ represents the $N_t \times N_r$ MIMO channel for the k th subcarrier and can be shown to be

$$\mathbf{H}(k) = \sum_{l=0}^{L-1} \mathbf{G}(l) \exp\left(-j2\pi \frac{kl}{N_c}\right) \quad (3)$$

where the l th path of MIMO CIR matrix $\mathbf{G}(l) \in \mathbb{C}^{N_r \times N_t}$ and its (q, p) th element is $g_{q,p}(l)$. We assume that these taps are independent, zero-mean, complex Gaussian random variables with variance $0.5P_l$ per dimension. The ensemble P_l , $l =$

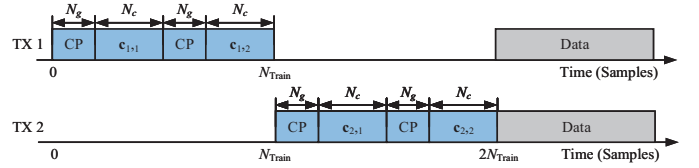


Fig. 1. Structure of a time orthogonal preamble for a 2×2 MIMO-OFDM system.

$\{0, \dots, L-1\}$ is called the power delay profile (PDP) and its total power is assumed to be normalized to $\sigma_c^2 = 1$. For each k th subcarrier, the signal model can be written in its flat-fading form as

$$\mathbf{x}(k, a) = \mathbf{H}(k) \mathbf{s}(k, a) + \mathbf{n}(k, a). \quad (4)$$

III. TRADITIONAL TIMING AND FREQUENCY SYNCHRONIZATION FOR MIMO-OFDM

We consider the traditional preamble pattern [4] and synchronization method [5] in this section. As shown in Fig. 1, in order to estimate the subchannels between the different TX and RX antennas, a time orthogonal preamble is chosen. The length of the preamble for all the TX antennas is $N_{\text{train}} = 2(N_g + N_c)$, where N_g and N_c denote the length of the cyclic prefix (CP) and one OFDM symbol, respectively. $\mathbf{c}_{p,1}$ and $\mathbf{c}_{p,2}$ are different pseudo-noise (PN) sequences transmitted by the p th TX.

The first part of the preamble $\mathbf{c}_{p,1}$ comprises two identical halves in the time domain, which are used for symbol timing and fractional CFO estimation. This kind of time-domain identical structure can be obtained by transmitting a PN sequence only on the even frequencies while zeros are placed on the odd frequencies. The second part of the preamble $\mathbf{c}_{p,2}$ contains a PN sequence on its odd frequencies to measure these subchannels and another PN sequence on the even frequencies to help determine the frequency offset.

A. Timing Synchronization

Before the estimation of the CFO is conducted, the STO (τ) needs to be estimated. The method for timing synchronization is given by [4], [5]

$$\hat{\tau} = \underset{d}{\operatorname{argmax}} \frac{1}{N_g} \sum_{m=0}^{N_g-1} \left[\frac{\sum_{p=1}^{N_t} |\Lambda(d_p + m)|^2}{\sum_{p=1}^{N_t} P(d_p + m)^2} \right], \quad (5)$$

where $d_p = d - (N_t - p)N_{\text{train}}$ and d are discrete variables. $\Lambda(d)$ is the complex autocorrelation of the first part of preamble \mathbf{c}_1 , and is given by

$$\Lambda(d) = \sum_{i=d-(N_c/2-1)}^d \sum_{q=1}^{N_r} r_q^*(i - N_c/2) r_q(i) \quad (6)$$

with $r_q(i)$ the i th sample of the received signal on the q th antenna. The received energy for the second half-symbol of \mathbf{c}_1 , $P(d)$, is defined by

$$P(d) = \sum_{i=d-(N_c/2-1)}^d \sum_{q=1}^{N_r} r_q^*(i) r_q(i). \quad (7)$$

Note that d is a time index corresponding to the first sample in a window of N_c samples.

B. Frequency Synchronization

In this subsection, the CFO estimation method is based on [4]. We define a normalized CFO, ε , as a ratio of the CFO f_{offset} to subcarrier spacing Δf , given as $\varepsilon = f_{\text{offset}}/\Delta f$. Let ε_i and ε_f denote the integer part and fractional part of ε , respectively, and therefore $\varepsilon = \varepsilon_i + \varepsilon_f$, where $\varepsilon_i = \lfloor \varepsilon \rfloor$. If $|\varepsilon| \leq 1$, the CFO can be estimated directly as

$$\hat{\varepsilon} = \frac{\hat{\theta}}{\pi} = \frac{\angle \left[\sum_{p=1}^{N_t} \Lambda(\hat{\tau}_p) \right]}{\pi}, \quad (8)$$

where $\hat{\tau}_p = \hat{\tau} - (N_t - p)N_{\text{train}}$ and $\hat{\theta}$ denotes the phase of the summation of the complex correlations of the preambles originating from the different transmitters. When $|\varepsilon| > 1$, the PN sequence on the even frequencies of \mathbf{c}_2 will be needed and the CFO can be given by

$$\varepsilon = \frac{\theta}{\pi} + 2g, \quad (9)$$

where g is an integer. By partially correcting the frequency offset, adjacent carrier interference can be avoided, and then the remaining offset of $2g$ can be found. In order to estimate g , the received preamble at the q th RX antenna from the p th TX antenna, corresponding to $\mathbf{c}_{p,1}$ and $\mathbf{c}_{p,2}$ needs to be frequency compensated by $\hat{\theta}$ at first and then transformed into the frequency domain as $\mathbf{x}_{q,p,1}$ and $\mathbf{x}_{q,p,2}$, respectively. Then, g can be estimated by the difference correlation as follows:

$$\hat{g} = \arg \max_g \frac{\sum_{p=1}^{N_t} \sum_{q=1}^{N_r} \left| \sum_{k \in X_{\text{Even}}} X_{q,p,1}^*[k+2g] v_p^*[k] X_{q,p,2}[k+2g] \right|^2}{2 \sum_{p=1}^{N_t} \sum_{q=1}^{N_r} \left(\sum_{k \in X_{\text{Even}}} |X_{q,p,2}[k]|^2 \right)^2}, \quad (10)$$

where X_{Even} represents the subset of even frequency indices and $v_p[k] = \sqrt{2}c_{p,2}[k]/c_{p,1}[k]$, $k \in X_{\text{Even}}$. Finally, the estimate can be written as

$$\hat{\varepsilon} = \frac{\hat{\theta}}{\pi} + 2\hat{g}. \quad (11)$$

IV. ELM-BASED RSTO AND RCFO ESTIMATION

Due to the fading channel and thermal noise, small but significant RSTO and RCFO will always exist to degrade the performance of MIMO-OFDM systems. In order to perform synchronization more accurately, the methods of ELM-based RSTO and RCFO estimations will be introduced in this section.

A. ELM-Based RSTO Estimation

Inspired by the idea that a neural network (NN) can learn from appropriate data, we try to further exploit (by a NN) the implicit information inside the preamble to estimate RSTO and RCFO. Compared with a DNN, an ELM only has single hidden layer and thus it has lower computational complexity,

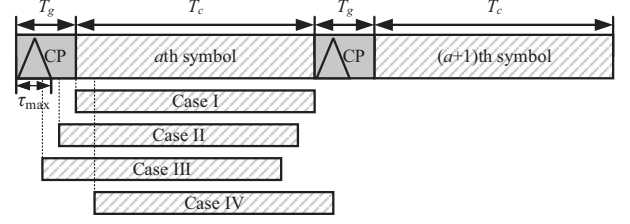


Fig. 2. Four different cases of an OFDM symbol starting point subject to STO.

but it still has excellent performance [26]. Specifically, the ELM model is chosen by comparing it with other machine learning models that are applied for communications signal processing in recent literature, mainly including DNN and CNN. Both DNN and CNN are typical deep learning technique, while ELM has a very simple network structure and is the most promising technique to reduce the required training data and computational complexity, which contributes to reduce latency. In that regard, we choose to employ ELM models in this paper. Specifically and most importantly, we expect that the relationships between the corrupted preamble signal and synchronization offset can be “learnt” by the ELM. Therefore, it is necessary to first explain the effect of STO.

Depending on the location of the estimated starting point of an OFDM symbol, the effect of STO can vary. Fig. 2 shows four different cases of timing offset, in which the estimated starting point is perfectly accurate (**Case I**), a little early (**Case II**), too early (**Case III**), or a little late compared to exact timing (**Case IV**). T_c , T_g and τ_{max} represent the duration of the OFDM symbol, the CP and the maximum excess delay, respectively [27].

In **Case II**, the channel response to the $(a-1)$ th OFDM symbol does not overlap with the a th OFDM symbol and so does not incur any ISI from the previous symbol. In this case, the received signal in the frequency domain is obtained by taking the FFT of the time domain received samples:

$$\mathbf{x}(k, a) = \mathbf{H}(k) \mathbf{s}(k, a) e^{j2\pi k\tau/N} + \mathbf{n}(k, a), \quad (12)$$

where τ denotes the STO. Equation (12) implies that the orthogonality among subcarrier frequency components can be completely preserved. However, there exists a phase offset that is proportional to the STO τ and subcarrier index k , forcing the signal constellation to be rotated around the origin in the complex plane.

In **Case III** and **Case IV**, the orthogonality among subcarrier components is destroyed by the ISI from the previous and the succeeding OFDM symbols, respectively. In addition, ICI will occur. A quantitative analysis of the ISI and ICI resulting from STO has been exhaustively studied in [27].

In order to avoid the occurrence of the **Case IV** in Fig. 2, the timing point will be set $N_g/4$ points ahead of the estimated value from the traditional estimator in the case of a fading

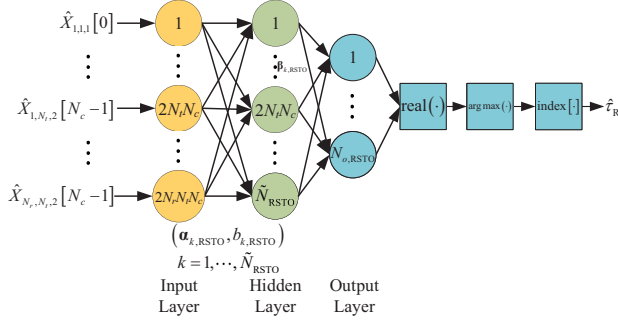


Fig. 3. The structure of an ELM-based RSTO estimator.

channel,¹ whereas it still cannot entirely eliminate the RSTO.

Therefore, a natural idea is that using ELM to learn the relationship between received preamble with ISI, ICI and RSTO τ_R , where $\tau_R = \tau - \hat{\tau}$. Compared with DNN, ELM is considered as a general form of single layer feedforward neural networks, where the input weights and hidden layer biases of ELM are randomly generated. In other words, hidden layer outputs are always known. Hence, this structure allows the analytical calculation of the output weights during the training phase by means of least square solutions. As a result, ELM has a competitive advantage in terms of computational complexity.

Under most situations, the starting point of an OFDM symbol will be one of the above-mentioned four cases. In other words, the probability of $|\tau_R| > N_g$ is very low, and this fact, is very important to the generation of the training set for ELM-based RSTO estimator. Specifically, the range of the target values (RSTO) should be set properly but not too small or large. Otherwise, an inappropriate training set leads to poor performance of the ELM model. The details about the ELM-based model for RSTO estimation and the generation of training set is given as follows.

The structure of a complex ELM-based RSTO estimator is illustrated in Fig. 3. The ELM-based RSTO estimator has $2N_r N_t N_c$ input neurons, \tilde{N}_{RSTO} hidden neurons and $N_{o,RSTO}$ output neurons. The input, output and weights of ELM can be fully complex. $\hat{X}_{q,p,i}[k]$ is the input in the prediction stage, which denotes the equalized frequency domain received signal at the q th RX antenna from the p th TX antenna corresponding to $\mathbf{c}_{p,i}$. The $\text{real}(\cdot)$ block returns the real part of the elements of the complex array and the $\text{argmax}(\cdot)$ block returns the indices of the maximum values. The principle of the ELM-based RSTO estimator can be divided into two main stages: training and prediction stages.

1) *Training Stage*: In this stage, the training set $\mathbf{N}_{RSTO} = \{(\tilde{\mathbf{X}}_n, \mathbf{O}_{n,RSTO}) | n = 1, \dots, N_{RSTO}\}$ is first generated. The n th input data of training set $\tilde{\mathbf{X}}_n \in \mathbb{C}^{2N_r N_t N_c \times 1}$ is given as

$$\tilde{\mathbf{X}}_n = \text{FFT}(\text{RemoveCP}(\mathbf{X}_n)), \quad (13)$$

where $\tilde{\mathbf{X}}_n$ denotes the combination vector of the preamble signal in the frequency domain by taking the FFT of the

time domain received samples with corresponding RSTO. In Equation (13), the pseudo-function “RemoveCP” and “FFT” represent respectively removing all the CPs and taking the N_c -point fast Fourier transform. Specifically, the time domain received samples with RSTO $\tau_{R,n}$ can be expressed as

$$\mathbf{X}_n = \tilde{\mathbf{c}}[k] \otimes \delta[k - \tau_{R,n}], \quad (14)$$

where

$$\tilde{\mathbf{c}} = [\tilde{\mathbf{c}}_1^T, \dots, \tilde{\mathbf{c}}_p^T, \dots, \tilde{\mathbf{c}}_{N_t}^T]^T, \quad (15)$$

and

$$\tilde{\mathbf{c}}_p = \text{repmat}\left(\left[\text{CP}_{\mathbf{c}_{p,1}}^T, \mathbf{c}_{p,1}^T, \text{CP}_{\mathbf{c}_{p,2}}^T, \mathbf{c}_{p,2}^T\right]^T, N_r, 1\right). \quad (16)$$

Note that, in Equation (14), $\delta[k - \tau_{R,n}]$ denotes a delayed Kronecker delta function. The absent elements of $\tilde{\mathbf{c}}$ will be filled by zero padding.

The n th target output, $\mathbf{O}_{n,RSTO}$ is a one-hot vector including encoded information of corresponding RSTO $\tau_{R,n}$. Now, for example, $[1, 0, \dots, 0]^T$ represents $\tau_R = -N_g$, $[0, \dots, 0, 1]^T$ represents $\tau_R = N_g$ and

$$\tau_{R,n} = \text{index} \left[\arg \max_{1 \leq i \leq 2N_g+1} (o_{n,RSTO,i}) \right], \quad (17)$$

where $\mathbf{O}_{n,RSTO} = [o_{n,RSTO,1}, o_{n,RSTO,2}, \dots, o_{n,RSTO,2N_g+1}]^T$. Here “index” represents an index array including different values of RSTO. In this paper, the size of the training set for the ELM-based RSTO estimator is $2N_g + 1$ and $\text{index} = [-N_g, \dots, N_g]$.

Then, the training set can be used for the determination of the weights and biases of the ELM. In **step 1** of **Algorithm 1** (see later), the complex input weight $\alpha_{k,RSTO}$ and complex bias $b_{k,RSTO}$ (see also Fig.3) are generated from the uniform distribution $U(-0.1, 0.1)$, where $\alpha_{k,RSTO} \in \mathbb{C}^{2N_r N_t N_c \times 1}$ is the input weight vector connecting input neurons to the k th hidden neuron and $\alpha_{RSTO} = [\alpha_{1,RSTO}, \dots, \alpha_{k,RSTO}, \dots, \alpha_{\tilde{N}_{RSTO},RSTO}]$ and $\mathbf{b}_{RSTO} = [b_{1,RSTO}, \dots, b_{k,RSTO}, \dots, b_{\tilde{N}_{RSTO},RSTO}]$. Once the input weights and biases are chosen, the output of the hidden layer can be given by

$$\mathbf{D}_{\text{Training},RSTO} = g_c \left(\alpha_{RSTO}^T \tilde{\mathbf{X}} + \mathbf{b}_{RSTO} \right) \quad (18)$$

where $\tilde{\mathbf{X}} = [\tilde{\mathbf{X}}_1 \ \tilde{\mathbf{X}}_2 \ \dots \ \tilde{\mathbf{X}}_N] \in \mathbb{C}^{2N_r N_t N_c \times N}$.

We expect that the output of the ELM could be close to the target output \mathbf{O}_{RSTO} , so

$$\beta_{RSTO} \mathbf{D}_{\text{Training},RSTO} = \mathbf{O}_{RSTO}. \quad (19)$$

Generally, $\beta_{RSTO} = [\beta_{1,RSTO}, \dots, \beta_{k,RSTO}, \dots, \beta_{\tilde{N}_{RSTO},RSTO}] \in \mathbb{C}^{N_{o,RSTO} \times \tilde{N}_{RSTO}}$ and $\beta_{k,RSTO} = [\beta_{k,RSTO,1}, \beta_{k,RSTO,2}, \dots, \beta_{k,RSTO,N_{o,RSTO}}]^T \in \mathbb{C}^{N_{o,RSTO} \times 1}$, where $\beta_{k,RSTO}$ denotes the output weight vector connecting the k th hidden neuron and the output neurons and $N_{o,RSTO}$ denotes the number of output neurons. For the ELM-based RSTO estimator, $N_{o,RSTO} = 2N_g + 1$. Under the criterion of

¹In order to avoid ISI, the FFT window start position has to be put in advance of the estimated point obtained by the coarse STO estimation algorithm [13].

Algorithm 1 The Training Algorithm for an ELM-based RSTO Estimator

We are given a training set $\mathbf{N}_{\text{RSTO}} = \{(\tilde{\mathbf{X}}_n, \mathbf{O}_{n,\text{RSTO}}) | n = 1, \dots, N_{\text{RSTO}}\}$, complex activation function $g_c(\cdot)$, and hidden neuron number \tilde{N}_{RSTO} . $\tilde{\mathbf{X}}_n \in \mathbb{C}^{2N_r N_t N_c \times 1}$, $\mathbf{O}_{n,\text{RSTO}}$ is a one-hot vector and these two correspond to the input and desired output of the ELM-based RSTO estimator, respectively.

Step 1: Randomly choose the values of complex input weight $\alpha_{k,\text{RSTO}}$ and the complex bias $b_{k,\text{RSTO}}$, $k = 1, \dots, \tilde{N}_{\text{RSTO}}$.

Step 2: Calculate the complex hidden layer output matrix $\mathbf{D}_{\text{Training,RSTO}}$.

Step 3: Calculate the complex output weight β_{RSTO} using $\hat{\beta}_{\text{RSTO}} = \mathbf{O}_{\text{RSTO}} \mathbf{D}_{\text{Training,RSTO}}^\dagger$, where $\mathbf{O}_{\text{RSTO}} \in \mathbb{C}^{N_{o,\text{RSTO}} \times N_{\text{RSTO}}}$.

minimizing the squared errors, the least squares (LS) solution is given by

$$\begin{aligned} \hat{\beta}_{\text{RSTO}} &= \underset{\beta_{\text{RSTO}}}{\operatorname{argmin}} \|\beta_{\text{RSTO}} \mathbf{D}_{\text{Training,RSTO}} - \mathbf{O}_{\text{RSTO}}\| \\ &= \mathbf{O}_{\text{RSTO}} \mathbf{D}_{\text{Training,RSTO}}^\dagger. \end{aligned} \quad (20)$$

The training algorithm for an ELM-based RSTO estimator can be summarized as shown in **Algorithm 1**.

2) *Prediction (Estimation) Stage:* For an ELM-based RSTO estimator, we assume that LS channel estimation is used or the perfect CSI is known. Thus the equalized preamble can be given by²

$$\hat{X}_{q,p,i}[k] = X_{q,p,i}[k] / \mathbf{H}_{q,p,i}[k]. \quad (21)$$

The output of hidden layer can be calculated as

$$\mathbf{D}_{\text{Prediction,RSTO}} = g_c(\alpha_{\text{RSTO}}^T \hat{\mathbf{x}} + \mathbf{b}_{\text{RSTO}}) \quad (22)$$

where

$$\hat{\mathbf{x}} = [\hat{\mathbf{x}}_{1,1,1}^T, \hat{\mathbf{x}}_{1,1,2}^T, \dots, \hat{\mathbf{x}}_{N_t, N_r-1, 1}^T, \hat{\mathbf{x}}_{N_t, N_r-1, 2}^T, \hat{\mathbf{x}}_{N_t, N_r, 1}^T, \hat{\mathbf{x}}_{N_t, N_r, 2}^T]^T. \quad (23)$$

Note that the input, output and all the weights and biases of ELM in this paper are complex values but RSTO and RCFO are real values. Therefore, the operator $\operatorname{real}(\cdot)$ following the output of ELM is necessary. By expressing $\operatorname{real}(\hat{\beta}_{\text{RSTO}} \mathbf{D}_{\text{Prediction,RSTO}})$ as $\operatorname{real}(\hat{\beta}_{\text{RSTO}} \mathbf{D}_{\text{Prediction,RSTO}}) = [\hat{o}_{1,\text{RSTO}}, \hat{o}_{2,\text{RSTO}}, \dots, \hat{o}_{2N_g+1,\text{RSTO}}]^T$, the RSTO is given as

$$\hat{r}_R = \operatorname{index} \left[\arg \max_{1 \leq i \leq 2N_g+1} (\hat{o}_{i,\text{RSTO}}) \right]. \quad (24)$$

B. ELM-Based RCFO Estimation

²A minimum mean-square error (MMSE) channel estimator cannot be deployed before the STO is estimated because the STO can degrade the performance of the MMSE channel estimator [28]. However, the simulation results in Section V still include the ELM-based STO estimator with MMSE channel estimation. The introduction of the MMSE channel estimator is given in the next subsection.

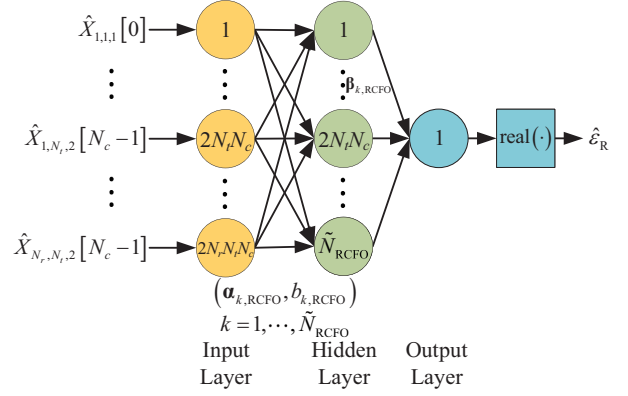


Fig. 4. The structure of an ELM-based RCFO estimator.

Algorithm 2 The Training Algorithm for an ELM-based RCFO Estimator

We are given a training set $\mathbf{N}_{\text{RCFO}} = \{(\tilde{\mathbf{I}}_n, O_{n,\text{RCFO}}) | n = 1, \dots, N_{\text{RCFO}}\}$, complex activation function $g_c(\cdot)$, and hidden neuron number \tilde{N}_{RCFO} . $\tilde{\mathbf{I}}_n \in \mathbb{C}^{2N_r N_t N_c \times 1}$, $O_{n,\text{RCFO}}$ is a real number and these two correspond to the input and desired output of the ELM-based RCFO estimator, respectively. Here, $O_{n,\text{RCFO}}$ denotes a given RCFO.

Steps 1, 2 and 3: Refer to **Algorithm 1**.

As Fig. 4 illustrates, the ELM-based RCFO estimator has $2N_r N_t N_c$ input neurons, \tilde{N}_{RCFO} hidden neurons and only one output neuron. Here, we use ε_R to denote the RCFO, where $\varepsilon_R = \varepsilon - \hat{\varepsilon}$.

1) *Training Stage:* Before ELM can be deployed to estimate RCFO, it has to learn the prior knowledge from the training set. The training algorithm for an ELM-based RCFO estimator can be summarized as shown in **Algorithm 2**.

Specifically, the n th input data of training set is given as

$$\tilde{\mathbf{I}}_n = \text{FFT}(\text{RemoveCP}(\mathbf{I}_n)), \quad (25)$$

where $\tilde{\mathbf{I}}_n$ denotes the combination vector of the preamble signal in the frequency domain by taking the FFT of the time domain received samples with corresponding RCFO, $\varepsilon_R = O_{n,\text{RCFO}}$. The time domain received samples with RCFO $O_{n,\text{RCFO}}$ can be expressed as

$$\mathbf{I}_n = [\tilde{\mathbf{c}}_1^T, \dots, \tilde{\mathbf{c}}_p^T, \dots, \tilde{\mathbf{c}}_{N_t}^T]^T \odot [\tilde{\mathbf{o}}_1^T, \dots, \tilde{\mathbf{o}}_p^T, \dots, \tilde{\mathbf{o}}_{N_t}^T]^T, \quad (26)$$

where

$$\tilde{\mathbf{c}}_p = \text{repmat} \left(\left[\text{CP}_{\mathbf{c}_{p,1}}^T, \mathbf{c}_{p,1}^T, \text{CP}_{\mathbf{c}_{p,2}}^T, \mathbf{c}_{p,2}^T \right]^T, N_r, 1 \right), \quad (27)$$

$$\tilde{\mathbf{o}}_p = \text{repmat}(\mathbf{o}_p, N_r, 1), \quad (28)$$

and

$$\mathbf{o}_p = \begin{bmatrix} e^{2\pi j[1+2(p-1)(N_c+N_g)]O_{n,\text{RCFO}}/N_c} \\ \vdots \\ e^{2\pi j[2(N_c+N_g)+2(p-1)(N_c+N_g)]O_{n,\text{RCFO}}/N_c} \end{bmatrix}. \quad (29)$$

In **step 1** of **Algorithm 2**, the generation of the input weight $\alpha_{k,\text{RCFO}}$ and bias $b_{k,\text{RCFO}}$ are the same as **step 1** in **Algorithm 1**. The output of the hidden layer can be given by

$$\mathbf{D}_{\text{Training,RCFO}} = g_c \left(\alpha_{\text{RCFO}}^T \tilde{\mathbf{I}} + \mathbf{b}_{\text{RCFO}} \right), \quad (30)$$

where $\tilde{\mathbf{I}} = [\tilde{\mathbf{I}}_1 \quad \tilde{\mathbf{I}}_2 \quad \cdots \quad \tilde{\mathbf{I}}_N] \in \mathbb{C}^{2N_r N_t N_c \times N}$.

We would expect that the output of the ELM could be close to the target output \mathbf{O}_{RCFO} , so $\beta_{\text{RCFO}} \mathbf{D}_{\text{Training,RCFO}} = \mathbf{O}_{\text{RCFO}}$. For the ELM-based RCFO estimator, $N_{o,\text{RCFO}} = 1$. The LS solution is then given by

$$\hat{\beta}_{\text{RCFO}} = \mathbf{O}_{\text{RCFO}} \mathbf{D}_{\text{Training,RCFO}}^\dagger. \quad (31)$$

2) *Prediction (Estimation) Stage*: Since the received preambles have been corrupted by the fading channel, channel estimation and equalization need to be carried out. Now that $\mathbf{c}_{p,2}$ is known and fully occupies the subcarriers, the minimum mean-square error (MMSE) estimate of the frequency impulse response [28] from the p th TX antenna to the q th RX antenna is given by

$$[\hat{\mathbf{H}}_{q,p}[0], \dots, \hat{\mathbf{H}}_{q,p}[N_c - 1]]^T = \mathbf{F} \mathbf{Q}_{\text{MMSE}} \mathbf{F}^H \mathbf{c}_{q,p,2}^H \mathbf{x}_{q,p,2}, \quad (32)$$

where \mathbf{Q}_{MMSE} can be shown to be

$$\mathbf{Q}_{\text{MMSE}} = \mathbf{R}_{\text{gg}} \left[\left(\mathbf{F}^H \mathbf{c}_{q,p,2}^H \mathbf{c}_{q,p,2} \mathbf{F} \right)^{-1} \sigma_n^2 + \mathbf{R}_{\text{gg}} \right]^{-1} \times \left(\mathbf{F}^H \mathbf{c}_{q,p,2}^H \mathbf{c}_{q,p,2} \mathbf{F} \right)^{-1}. \quad (33)$$

\mathbf{R}_{gg} is the auto-covariance matrix of $[g_{q,p}(0), \dots, g_{q,p}(L-1)]^T$ for any (q,p) . In other words, all the auto-covariance matrices of subchannels are the same. σ_n^2 denotes the noise variance $\mathbb{E}\{[n_k^2]\}$. Here, we assume that the auto-covariance matrices of all the subchannels between the TX antennas and the RX antennas are the same, so the subscripts of \mathbf{R}_{gg} are omitted. Then, the equalized preamble can be given by

$$\hat{X}_{q,p,i}[k] = X_{q,p,i}[k] / \hat{\mathbf{H}}_{q,p,i}[k]. \quad (34)$$

The calculation of the output of the hidden layer and $\hat{\mathbf{x}}$ are same as Equations (22) and (23), respectively. Finally, the RCFO is estimated as

$$\hat{\varepsilon}_R = \text{real} \left(\hat{\beta}_{\text{RCFO}} \mathbf{D}_{\text{Prediction,RCFO}} \right). \quad (35)$$

C. Complexity Analysis

We use the number of complex multiplications (CMs) to measure the computational complexity. For simplicity, the numbers of CMs for calculating the Moore-Penrose pseudoinverse of an $I \times O$ matrix is denoted as $C_{\text{pinv}}(OI^2)$. We compare the proposed complex ELM-based method with the DNN-based method. We assume that the input and output dimensions of the complex ELM-based method are I and O , respectively. For a DNN-based method, we split a complex number into a real part and an imaginary part. Thus, the input and output dimensions of the DNN-based method are $2I$ and $2O$, respectively. In the DNN-based method, there are real-valued multiplications. When calculating the computational

TABLE I
COMPARISON OF COMPLEXITY IN THE ESTIMATION STAGE

Methods	Numbers of Multiplications
Traditional [4], [5]	$N_t N_r N_c$ per metric calculation
DNN-based	$N_t N_r N_c$ per metric calculation + $IO \sum_{l=1}^{N_l} n_l n_{l-1}$
ELM-based	$N_t N_r N_c$ per metric calculation + ION

complexity, we consider that four real-valued multiplications are equivalent to one CM.

The machine learning-based method has two phases, i.e., the training phase and the prediction (estimation) phase, and we analyze the computational complexity for the two phases individually.

As for the training phase, the calculation of the output weights of complex ELM-based method requires $C_{\text{pinv}}(N\tilde{N}^2) + N(\tilde{N} + O)$ CMs where N is the number of training samples. The training complexity of the DNN-based method is difficult to derive using the number of CMs because it is trained iteratively with forward propagation (FP) and backpropagation (BP). Generally, the training complexity of the DNN is obviously higher than the complex ELM, and so the time consumption in training means it is difficult to satisfy the latency constraint in practical use cases.

The required numbers of CMs for the estimation phase are summarized in Table I, where N_l and n_l denote the number of hidden layers and the number of neurons at the l th hidden layer, respectively. \tilde{N} is the number of hidden neurons in the complex ELM. As can be seen, the proposed method has a significantly lower computational complexity compared to the DNN-based method and only requires ION extra CMs compared to the traditional method.

Different from the stage of training, it should be noticed that the input of the ELM in the prediction stage is the preamble corrupted by RSTO, RCFO, multipath fading channel and thermal noise. Therefore, the only question is whether the proposed method can outperform the traditional method. The following subsection will provide exhaustive simulation results and comparisons.

V. SIMULATION RESULTS AND COMPARISONS

In this section, the simulation setup is provided in detail and then, the performance of the proposed ELM-based RSTO and RCFO estimators is demonstrated.

A. Simulation Setup

1) *System Parameters and Channel Model*: For the numerical simulations, we set $N_c = 64$, $N_g = N_c/4$ and sampling frequency $f_s = 4 \times 10^6$. The wireless fading channel is modeled as an exponential model and quasistatic assumption is guaranteed during each OFDM symbol. For an exponentially decaying PDP, the root mean square (RMS) delay spread $\tau_{\text{RMS}} = 2 \times 10^{-6}$ s, and the coherence bandwidth $B_c = 1/\tau_{\text{RMS}} = 5 \times 10^5$ Hz. The PDP is given by

$$P_l = \exp \left(\frac{-2\pi B_c \tau_l}{\sqrt{3}} \right) \quad (36)$$

where the delay of l th path is set as $\tau_l = lT_s$ and $L = 8$.

TABLE II
PARAMETERS OF TRAINING SETS AND \tilde{N} FOR DIFFERENT MIMO SYSTEMS

MIMO System	Range of RSTO	Interval of RSTO	\tilde{N}_{RSTO}
2×2	$[-N_g, N_g]$	1	2^{14}
MIMO System	Range of RCFO	Interval of RCFO	\tilde{N}_{RCFO}
1×1	$[-0.0025, 0.0025]$	5.0×10^{-6}	2^{11}
2×2	$[-0.0025, 0.0025]$	2.5×10^{-6}	2^{14}
3×3 (Fading)	$[-0.0030, 0.0030]$	5.0×10^{-6}	2^{17}
3×3 (AWGN)	$[-0.05, 0.05]$	1.0×10^{-4}	2^{17}
4×4 (Fading)	$[-0.0010, 0.0010]$	1.0×10^{-5}	2^{14}
4×4 (AWGN)	$[-0.05, 0.05]$	5.0×10^{-4}	2^{14}

In addition, for a fair comparison, we keep the total transmitting power the same as in the single-input single-output (SISO) case. Therefore, the power per TX antenna is scaled down by a factor N_t .

2) *Training Sets, Hyperparameters and Activation Function*: The performance of a NN is usually sensitive to the training set, activation function and hyperparameters. Therefore, for an ELM-based RSTO and a RCFO estimators, the range and interval of the desired output in a training set should be chosen carefully. Generally, the power of a channel path with large delay is usually very low and therefore it may not significantly degrade the performance of timing synchronization. So we set the range of RSTO of training from $-N_g$ to N_g . Besides, the variance of the traditional CFO estimator decreases as N_r increases. We also have observed that adjusting the range and interval of RCFO in a training set affects the performance of the ELM-based RCFO estimator. So we generate different training sets and use the method of grid search to choose the best one among them. The training sets for different MIMO systems are summarized in Table II. The number of hidden neurons \tilde{N} is selected by the same method. Moreover, \tilde{N} must be larger than or equal to the size of a training set N so that the capacity of an ELM is high enough to learn the training set [29]. We choose $g_c(z) = \text{arcsinh}(z) = \int_0^z dt / \sqrt{1+t^2}$, where $z \in \mathbb{C}$ as the complex activation function, because arcsinh performs very well in certain learning environments due to its elegant symmetric and “squashing” magnitude responses [30].

B. Performance of the ELM-based RSTO Estimator

As it is instructive to observe the mean bias error (MBE) as well as the MSE of an estimator (where $\text{MSE} = \text{variance} + (\text{bias})^2$), we will examine both the bias and the MSE of the proposed estimator and compare this with the traditional estimator.

In Fig. 5, the MBE of the STO estimation is illustrated as a function of the average SNR per receive antenna. The results from Monte Carlo simulations averaged over 3×10^5 channel realizations are shown. In the cases of both an AWGN channel and a frequency-selective fading channel with perfect CSI information, it can be seen that the proposed ELM-based estimator has a much smaller bias than the traditional estimator. The MBE of ELM-based estimator approaches zero when $\text{SNR} \geq 3$ dB. In the cases of a frequency-selective fading

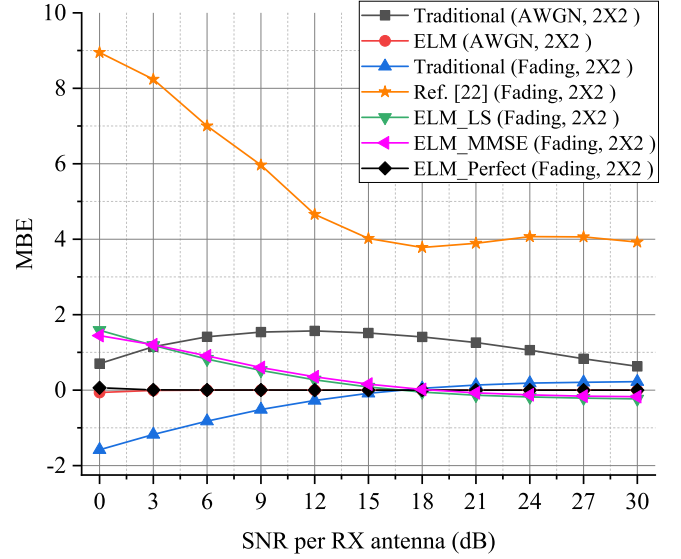


Fig. 5. MBE performance comparison between the traditional STO estimator, ELM-based estimator in [22] and the proposed ELM-based STO estimator for a 2×2 system with AWGN and a multipath fading channel.

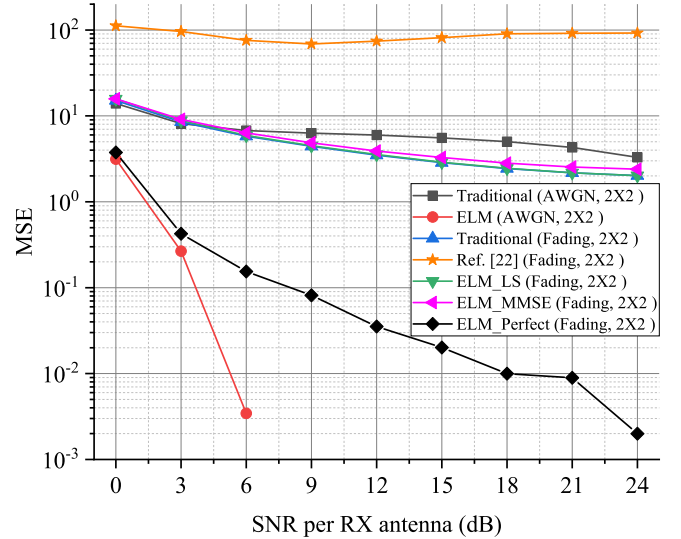


Fig. 6. MSE performance comparison between the traditional STO estimator, ELM-based estimator in [22] and the proposed ELM-based STO estimator for a 2×2 system with AWGN and a multipath fading channel.

channel with LS and MMSE channel estimation, the proposed ELM-based STO estimator does not show a gain in terms of MBE. This is because the imperfect channel estimation leads to the error of timing metric. In addition, the MBE of a recent ELM-based estimator proposed in [22] is obviously higher than other estimators even at a relatively high SNR because the method of the generation of training data in [22] relies on a given channel model and therefore makes it impractical.

In Fig. 6, the MSE of the STO estimation is displayed as a function of the average SNR per receive antenna. It can be seen that the proposed ELM-based estimator has a significantly smaller MSE than the traditional estimator and the ELM-based estimator in [22] in the cases of both an AWGN channel and a frequency-selective fading channel with

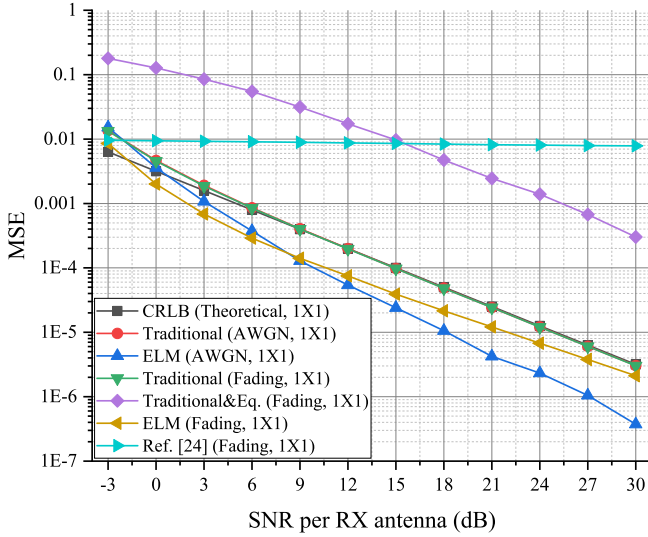


Fig. 7. MSE performance comparison between the traditional CFO estimator, DNN-based estimator in [24] and the proposed ELM-based CFO estimator for an 1×1 system from theory and simulations with AWGN and a multipath fading channel.

perfect CSI information. Even if the proposed ELM-based estimator acquires the imperfect CSI just by using a LS or an MMSE channel estimate, the MSE performance of the proposed ELM-based STO estimator is much better than the ELM-based estimator in [22]. It shows that the proposed method can learn the RSTO based on training data and then predict it very well.

C. Performance of the ELM-based RCFO Estimator

For the estimation of CFO, the performance of the estimator based on the traditional method and its Cramér-Rao lower bound (CRLB) will also be studied and used as a benchmark. Note that the CRLB is equal to the variance of traditional CFO estimator [5]

$$\text{var}(\hat{\varepsilon} - \varepsilon) = \frac{1}{\pi^2 N_t N_r V \rho} \quad (37)$$

where V is the length of identical halves in the first part of the preamble and $\rho = (P/N_t)\sigma_n^2$ denotes the SNR per receive antenna when the preamble is transmitting and P is the total transmit power.³ Note that (37) is approximately accurate under the condition of small errors ($\hat{\varepsilon} - \varepsilon$) and high SNR and it is derived in the appendix. We assume that timing synchronization is perfect ($\hat{\tau} = \tau$) when the performances of both the traditional and the ELM-based CFO estimators are evaluated.

1) *MSE Performance*: In Fig. 7, the MSE of the CFO estimation is demonstrated as a function of the average SNR per receive antenna. The theoretical value from (37) is shown together with results from Monte Carlo simulations averaged over 10^5 channel realizations. As seen from Fig. 7, the MSE curve of the traditional method almost perfectly overlaps that of the CRLB. The theoretical value is a good estimate of

³(37) also can be written as $\text{var}(\hat{\varepsilon} - \varepsilon) = \frac{1}{\pi^2 N_r V \rho'}$, where the SNR per receive antenna is defined as $\rho' = P \sigma_n^2$.

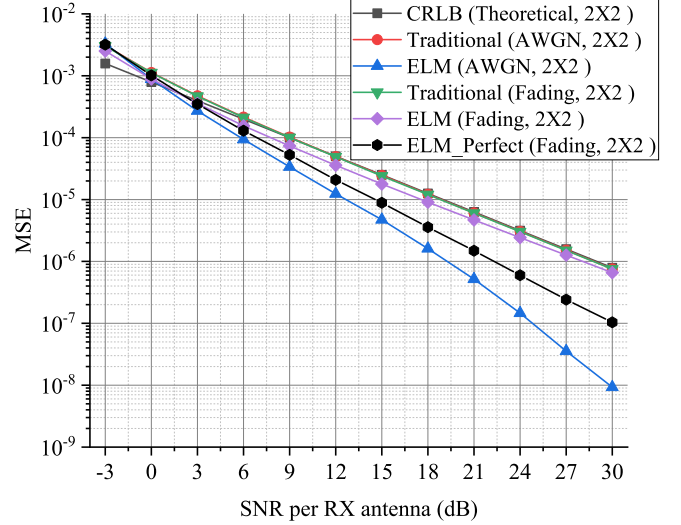


Fig. 8. MSE performance comparison between the traditional CFO estimator and the proposed ELM-based CFO estimators for a 2×2 system from theory and simulations with AWGN and a multipath fading channel.

the MSE for high SNR values but underestimates the MSE compared with simulation results for low SNR. Note that the CRLB expresses a lower bound on the variance of unbiased estimators of a deterministic parameter. A biased approach can result in both a variance and a MSE that are below the unbiased CRLB. Specifically, in the case of AWGN, when $\text{SNR} = -3$ dB, ELM obtains a slightly larger MSE value compared with simulation results for the traditional method. Fortunately, we can see that the performance improvement between ELM and the traditional method increases with SNR, and when $\text{SNR} = 21$ dB ELM achieves a SNR gain of about 9 dB over the traditional method at a MSE value of 4.22×10^{-6} . In the case of a frequency-selective fading channel, the largest SNR gain over a traditional method, about 4.5 dB, is achieved when $\text{SNR} = 6$ dB. This kind of the gain becomes insignificant when $\text{SNR} > 27$ dB.

We also use the DNN-based model and training method proposed in [24] to estimate RCFO. It can be seen that its MSE performance is significantly inferior to that of other methods and it does not have obvious change as SNR increases. This is because the channel impulse used for the generation of training set is different from the channel impulse of each channel realization, and therefore it leads to poor performance.

To provide further insights on the proposed method and prove that the gain of ELM is not just a result of channel estimation and equalization, the curve of “Traditional&Eq.” shows the MSE performance of the traditional method with channel estimation and equalization. Specifically, the method “Traditional&Eq.” performs traditional CFO estimation twice. The first CFO estimation uses the traditional method. Then, channel estimation and equalization are performed by using the frequency corrected preamble signal. Finally, the traditional CFO estimation method is performed again to estimate RCFO by using the frequency corrected and equalized preamble signal. It can be seen that its performance seriously degrades, which means that channel estimation and equaliza-

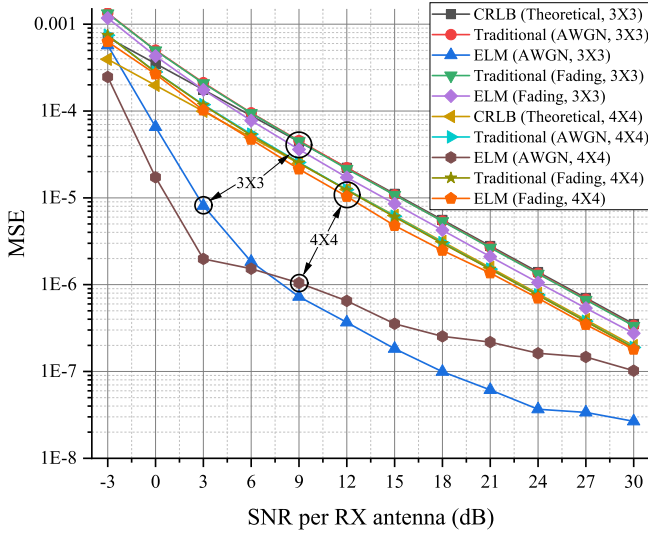


Fig. 9. MSE performance comparison between the traditional CFO estimator and the proposed ELM-based CFO estimator for a 3×3 and 4×4 systems from theory and simulations with AWGN and a multipath fading channel.

tion cannot enhance the performance of the traditional CFO estimator. This can be explained by the fact that the ELM can reuse the preamble exhaustively and also learn the mapping relationships between RCFOs and their corresponding preambles with RCFOs.

Fig. 8 presents the MSE curves of the traditional and proposed ELM-based CFO estimators for a 2×2 system. Similar to the observations in Fig. 7, in the case of an AWGN channel, the MSE performance of the ELM still outperforms that of the traditional method. Using the ELM, when SNR = 18 dB, about 9 dB SNR gain over traditional method is achieved at $\text{MSE} = 2.16 \times 10^{-6}$. In the case of a frequency-selective fading channel, by comparing Fig. 8 with Fig. 7, we find that the gains of ELM over the traditional method for a 2×2 system (about 1.5 dB) are lower than that for 1×1 system (about 1.5-4.5 dB). We conjecture that this is because the accuracy of channel estimation limits the CFO estimation performance of the ELM.

In order to prove this conjecture, we also perform the simulation for the ELM estimator with perfect channel state information (CSI). In Fig. 8, the curve “ELM_Perfect” illustrates the performance of the ELM with perfect CSI. It can be seen that, under the condition of knowing perfect CSI, the MSE performance of the ELM under the condition of fading channel is closer to that under the condition of AWGN channel compared to that of ELM without perfect CSI. The gain from perfect CSI increases with the increase of SNR. So we can conjecture that the performance of the ELM-based scheme is sensitive to the accuracy of the CSI.

Fig. 9 presents the MSE curves of the traditional and the proposed ELM-based CFO estimators for a 3×3 and 4×4 MIMO systems. Note that for the 3×3 and 4×4 systems, the ELM models are trained by different training sets separately in order to achieve the best performance under AWGN and fading channel conditions. In the case of an AWGN channel for the 3×3 system, when SNR = -3 dB, the MSE performance of the

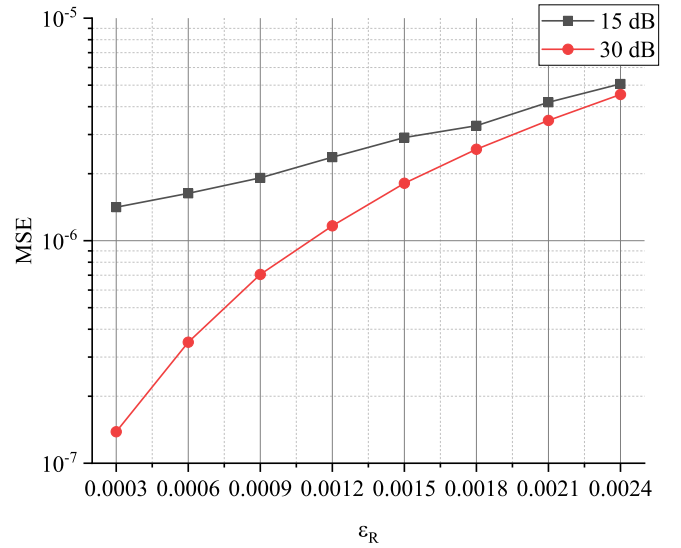


Fig. 10. MSE versus ϵ_R curves of the proposed ELM-based CFO estimator for a 2×2 system.

ELM is slightly better than the CRLB but its MSE decreases rapidly with an increase of SNR. When SNR = 12 dB, about 18 dB SNR gain over the traditional method is achieved by the ELM-based method. For the 4×4 system, ELM-based method achieves its highest gain (about 16.5 dB) over the traditional method. By comparing Fig. 9 with Fig. 8 and Fig. 7, the gain of the ELM-based method over the traditional method at low SNRs increases with the increase in the number of RX antennas. At high SNRs, the gains are not as high as the highest gains. This is because the MSE performance of the ELM relates to the number of the receive antennas, and the gain of ELM is from both noise suppression and mining information exhaustively from preambles. In the case of a frequency-selective fading channel for the both 3×3 and 4×4 systems, the ELM can obtain about 1.5 dB gain of MSE when SNR ≥ 3 dB, which is similar with the case for a 2×2 system.

2) *Robustness Analysis:* In this part, we analyze the robustness of the proposed ELM scheme. Fig. 10 shows the MSE of ELM under various RCFOs when SNR = 15 dB and 30 dB. It can be seen that the MSE increases with an increase of RCFO. By comparing Fig. 10 with Fig. 8, when SNR = 30 dB and $\epsilon_R \geq 0.0012$, the MSE of the ELM is higher than that in Fig. 8 ($\text{MSE} > 10^{-6}$). However, when SNR = 15 dB and $\epsilon_R \leq 0.0024$, the MSE of ELM is lower than that in Fig. 8 ($\text{MSE} < 10^{-5}$). This can be explained by the fact that the performance advantage and robustness of the ELM-based method are more significant in medium SNR.

Fig. 11 shows the MSE of the ELM under a channel with different number of channel paths when SNR = 15 dB and 30 dB. It can be seen that, with increase of L , the MSE of the ELM is almost unchanged, which means that the proposed method is robust enough to handle frequency-selective fading channels with different numbers of paths. The simulation results demonstrate the robustness of the proposed method to the RCFO and propagation environments.

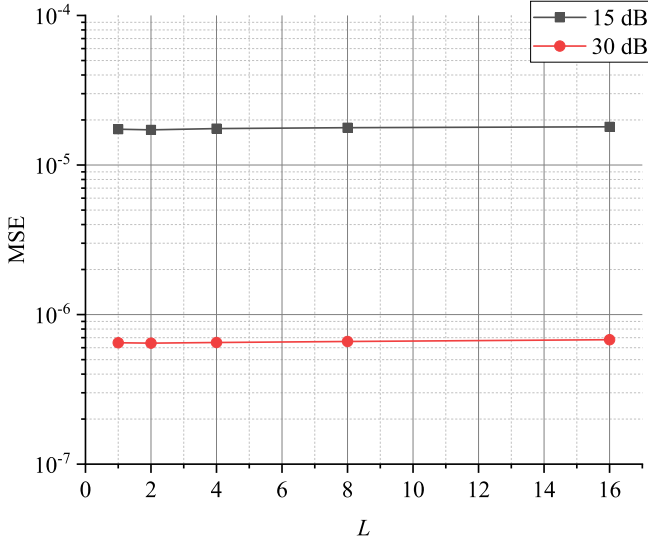


Fig. 11. MSE versus the number of paths of a fading channel (L) of the proposed ELM-based CFO estimator for a 2×2 system.

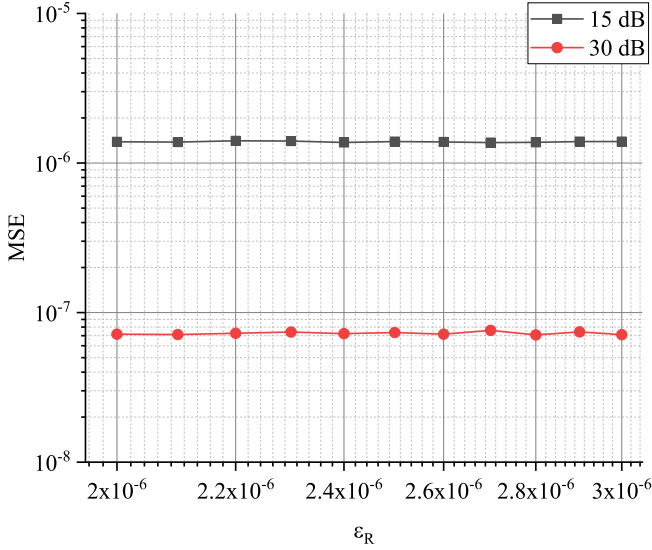


Fig. 12. MSE versus the RCFO not belonging to a training set of the proposed ELM-based CFO estimator for a 2×2 system.

3) *Generalization Error Analysis*: Generalization is a term used to describe the ability of a model to react to new data. That is, after being trained on a training set, can a model “digest” new data and make accurate predictions? In this paper, we also use MSE to evaluate the generalization ability of the ELM. Specifically, an RCFO not belonging to the training set is used to verify the generalization of a trained ELM-based RCFO estimator. The generalization ability of ELM can be analyzed according to Fig. 12, where we have used RCFOs that do not belong to the training set $O_{n,RCFO} \in \{2.5 \times 10^{-6}k | k = -1000, \dots, 1000\}$. By comparing Fig. 12 with Fig. 8, the performance of the ELM-based RCFO estimator does not change significantly when it handles those unfamiliar RCFOs. It can be concluded that the ELM-based RCFO estimator shows excellent generalization when it

processes an RCFO not belonging to the training set.

VI. CONCLUSIONS AND FUTURE WORK

In this paper, we have proposed an ELM-based fine timing and frequency synchronization scheme in order to improve the performance of existing estimators. The proposed scheme does not require any additional preamble and the training processes can be carried out fully offline without any prior information about the channels. Simulation results have shown that the proposed ELM-based synchronization scheme outperforms or achieves comparable performance in terms of MSE with existing traditional and learning-based synchronization algorithms. In addition, the proposed scheme shows robustness under various channels with different parameters and a generalization ability towards any RCFO outside the training set.

The simulation results have shown that the performance of the proposed ELM-based scheme relates to the accuracy of the CSI. Besides, it should be noticed that channel equalization can neutralize the effects of both STO and the fading channel. Therefore, this makes it difficult to obtain the received preamble signal affected by just the STO alone. In other words, the accurate CSI is still indispensable for the deployment of machine learning in communications systems. Therefore, incorporating ELM into transmitter design, synchronization and channel estimation and equalization jointly within system design is a promising future research direction.

APPENDIX A

VARIANCE OF THE CFO ESTIMATION FOR A MIMO SYSTEM UNDER AWGN CHANNEL (SEE (37))

We use the method in [3] and [31] to derive the variance of the CFO estimate for a MIMO system. According to (8), for a given ε , subtract the corresponding phase, $\pi\varepsilon$, from each product to obtain the tangent of the phase error

$$\tan[\pi(\hat{\varepsilon} - \varepsilon)] = \frac{\sum_{p=1}^{N_t} \sum_{q=1}^{N_r} \sum_{i=d_p-(V-1)}^{d_p} \text{Im}[r_q^*(i-V) r_q(i) e^{-\pi j \varepsilon}]}{\sum_{p=1}^{N_t} \sum_{q=1}^{N_r} \sum_{i=d_p-(V-1)}^{d_p} \text{Re}[r_q^*(i-V) r_q(i) e^{-\pi j \varepsilon}]}$$

(38)

where $d_p = d - (N_t - p)N_{\text{train}}$, V denotes the length of identical halves in the first part of the preamble and $r_q(i) = \tilde{r}_q(i) + n_q(i)$. $n_q(i)$ denotes the time domain noise of i th sample of the received signal on the q th antenna. For $|\hat{\varepsilon} - \varepsilon| \ll 1/\pi$, the tangent can be approximated by its argument so that

$$\hat{\varepsilon} - \varepsilon \approx \frac{\sum_{p=1}^{N_t} \sum_{q=1}^{N_r} \sum_{i=d_p-(V-1)}^{d_p} \text{Im}\{\tilde{r}_q(i-V) + n_q(i) e^{-\pi j \varepsilon}\} [\tilde{r}_q^*(i) + n_q^*(i) e^{-\pi j \varepsilon}]}{\pi \sum_{p=1}^{N_t} \sum_{q=1}^{N_r} \sum_{i=d_p-(V-1)}^{d_p} \text{Re}\{\tilde{r}_q(i-V) + n_q(i) e^{-\pi j \varepsilon}\} [\tilde{r}_q^*(i) + n_q^*(i) e^{-\pi j \varepsilon}]}$$

(39)

According to the method in [3], at high SNR, a condition compatible with successful communications signalling means that (39) may be approximated by

$$\hat{\varepsilon} - \varepsilon \approx \frac{\left\{ \sum_{p=1}^{N_t} \sum_{q=1}^{N_r} \sum_{i=d_p-(V-1)}^{d_p} \text{Im}[n_q(i) \tilde{r}_q^*(i-V) e^{-\pi j \varepsilon} + \tilde{r}_q(i-V) n_q^*(i-V)] \right\}}{\left\{ \pi \sum_{p=1}^{N_t} \sum_{q=1}^{N_r} \sum_{i=d_p-(V-1)}^{d_p} |\tilde{r}_q(i)|^2 \right\}}$$

(40)

It is easy to show that

$$E[\hat{\varepsilon} - \varepsilon | \varepsilon, \{\tilde{r}_q\}] = 0. \quad (41)$$

Therefore, for small errors, the estimate is conditionally unbiased. Then, the conditional variance of the estimate is easily determined for (40) as

$$\text{Var}[\hat{\varepsilon} | \varepsilon, \{\tilde{r}_q\}] = \frac{1}{\pi^2 N_t N_r V \rho}. \quad (42)$$

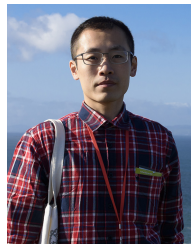
Finally, note that in this paper, $\rho = \sigma_{\tilde{r},q}^2 / \sigma_n^2 = (P/N_t) \sigma_n^2$ denotes the SNR per receive antenna when the preamble is transmitting and P is the total transmit power.

ACKNOWLEDGEMENT

The authors would like to acknowledge the help received from Longguang Wang. In addition, Jun Liu gratefully acknowledges the financial support received from the China Scholarship Council (CSC) and the School of Electronic and Electrical Engineering, University of Leeds, UK. He also wants to thank, in particular, the inspiration and care received from Yanling (Julia) Zhu during the period of this COVID-19 pandemic.

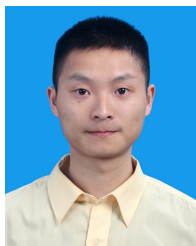
REFERENCES

- [1] N. Rajatheva, I. Atzeni, E. Bjornson, and et al., "White paper on broadband connectivity in 6G," *arXiv preprint arXiv:2004.14247*, 2020.
- [2] T. Balachander and M. M. Krishnan, "Carrier frequency offset (CFO) synchronization and peak average power ratio (PAPR) minimization for energy efficient cognitive radio network (CRN) for 5G wireless communication," *Wireless Personal Communications*, pp. 1–21, 2021.
- [3] P. H. Moose, "A technique for orthogonal frequency division multiplexing frequency offset correction," *IEEE Transactions on Communications*, vol. 42, no. 10, pp. 2908–2914, 1994.
- [4] T. M. Schmidl and D. C. Cox, "Robust frequency and timing synchronization for OFDM," *IEEE Transactions on Communications*, vol. 45, no. 12, pp. 1613–1621, 1997.
- [5] A. van Zelst and T. C. W. Schenk, "Implementation of a MIMO OFDM-based wireless LAN system," *IEEE Transactions on Signal Processing*, vol. 52, no. 2, pp. 483–494, 2004.
- [6] A. N. Mody and G. L. Stuber, "Synchronization for MIMO OFDM systems," in *GLOBECOM'01. IEEE Global Telecommunications Conference (Cat. No. 01CH37270)*, vol. 1, 2001, pp. 509–513 vol.1.
- [7] M. Ghogho and A. Swami, "Training design for multipath channel and frequency-offset estimation in MIMO systems," *IEEE Transactions on Signal Processing*, vol. 54, no. 10, pp. 3957–3965, 2006.
- [8] P. Cheng, Z. Chen, F. de Hoog, and C. K. Sung, "Sparse blind carrier-frequency offset estimation for OFDMA uplink," *IEEE Transactions on Communications*, vol. 64, no. 12, pp. 5254–5265, 2016.
- [9] M. Huang, L. Huang, C. Guo, P. Zhang, J. Zhang, and L. Yang, "Carrier frequency offset estimation in uplink OFDMA systems: An approach relying on sparse recovery," *IEEE Transactions on Vehicular Technology*, vol. 66, no. 10, pp. 9592–9597, 2017.
- [10] H. Abdzadeh-Ziabari, W. Zhu, and M. N. S. Swamy, "Joint maximum likelihood timing, frequency offset, and doubly selective channel estimation for OFDM systems," *IEEE Transactions on Vehicular Technology*, vol. 67, no. 3, pp. 2787–2791, 2018.
- [11] R. Shaked, N. Shlezinger, and R. Dabora, "Joint estimation of carrier frequency offset and channel impulse response for linear periodic channels," *IEEE Transactions on Communications*, vol. 66, no. 1, pp. 302–319, 2018.
- [12] A. A. Nasir, S. Durrani, H. Mehrpouyan, S. D. Blostein, and R. A. Kennedy, "Timing and carrier synchronization in wireless communication systems: a survey and classification of research in the last 5 years," *EURASIP Journal on Wireless Communications and Networking*, vol. 2016, no. 1, p. 180, 2016.
- [13] D. Chang, "Effect and compensation of symbol timing offset in OFDM systems with channel interpolation," *IEEE Transactions on Broadcasting*, vol. 54, no. 4, pp. 761–770, 2008.
- [14] M. M. U. Gul, X. Ma, and S. Lee, "Timing and frequency synchronization for OFDM downlink transmissions using Zadoff-Chu sequences," *IEEE Transactions on Wireless Communications*, vol. 14, no. 3, pp. 1716–1729, 2015.
- [15] R. C. Daniels, C. M. Caramanis, and R. W. Heath, "Adaptation in convolutionally coded MIMO-OFDM wireless systems through supervised learning and SNR ordering," *IEEE Transactions on vehicular Technology*, vol. 59, no. 1, pp. 114–126, 2009.
- [16] M. Sonal, "Machine learning for PAPR distortion reduction in OFDM systems," Master's thesis, School of Electrical Engineering, KTH Royal Institute of Technology, 2016.
- [17] T. Van Luong, Y. Ko, N. A. Vien, D. H. Nguyen, and M. Matthaiou, "Deep learning-based detector for OFDM-IM," *IEEE Wireless Communications Letters*, vol. 8, no. 4, pp. 1159–1162, 2019.
- [18] A. Li, Y. Me, S. Xue, N. Yi, and R. Tafazolli, "A carrier-frequency-offset resilient OFDMA receiver designed through machine deep learning," in *2018 IEEE 29th Annual International Symposium on Personal, Indoor and Mobile Radio Communications (PIMRC)*. IEEE, 2018, pp. 1–6.
- [19] Z. He and X. Huang, "Improved deep learning in OFDM systems with imperfect timing synchronization," in *2020 IEEE 91st Vehicular Technology Conference (VTC2020-Spring)*. IEEE, 2020, pp. 1–5.
- [20] S. Dörner, S. Cammerer, J. Hoydis, and S. t. Brink, "Deep learning based communication over the air," *IEEE Journal of Selected Topics in Signal Processing*, vol. 12, no. 1, pp. 132–143, 2018.
- [21] H. Wu, Z. Sun, and X. Zhou, "Deep learning-based frame and timing synchronization for end-to-end communications," in *Journal of Physics: Conference Series*, vol. 1169, no. 1, 2019, p. 012060.
- [22] C. Qing, W. Yu, B. Cai, J. Wang, and C. Huang, "ELM-based frame synchronization in burst-mode communication systems with nonlinear distortion," *IEEE Wireless Communications Letters*, vol. 9, no. 6, pp. 915–919, 2020.
- [23] M. Elwekeil, S. Jiang, T. Wang, and S. Zhang, "Deep convolutional neural networks for link adaptations in MIMO-OFDM wireless systems," *IEEE Wireless Communications Letters*, vol. 8, no. 3, pp. 665–668, 2018.
- [24] V. Ninkovic, D. Vukobratovic, A. Valka, and D. Dumic, "Deep learning based packet detection and carrier frequency offset estimation in IEEE 802.11ah," *arXiv preprint arXiv:2004.11716*, 2020.
- [25] C. E. Shannon, "A mathematical theory of communication," *The Bell System Technical Journal*, vol. 27, no. 3, pp. 379–423, 1948.
- [26] J. Liu, K. Mei, X. Zhang, D. Ma, and J. Wei, "Online extreme learning machine-based channel estimation and equalization for OFDM systems," *IEEE Communications Letters*, vol. 23, no. 7, pp. 1276–1279, jul 2019.
- [27] Y. S. Cho, J. Kim, W. Y. Yang, and C. G. Kang, *MIMO-OFDM wireless communications with MATLAB*. John Wiley & Sons, 2010.
- [28] J.-J. Van De Beek, O. Edfors, M. Sandell, S. K. Wilson, and P. O. Borjesson, "On channel estimation in OFDM systems," in *1995 IEEE 45th Vehicular Technology Conference. Countdown to the Wireless Twenty-First Century*, vol. 2. IEEE, 1995, pp. 815–819.
- [29] G.-B. Huang, "Learning capability and storage capacity of two-hidden-layer feedforward networks," *IEEE transactions on neural networks*, vol. 14, no. 2, pp. 274–281, 2003.
- [30] T. Kim and T. Adali, "Approximation by fully complex multilayer perceptrons," *Neural Computation*, vol. 15, no. 7, pp. 1641–1666, 2003.
- [31] T. Schenk, *RF imperfections in high-rate wireless systems: impact and digital compensation*. Springer Science & Business Media, 2008.



Jun Liu received the B.S. degree in optical information science and technology from the South China University of Technology (SCUT), Guangzhou, China, in 2015, and the M.E. degree in communications and information engineering from the National University of Defense Technology (NUDT), Changsha, China, in 2017, where he is currently pursuing the Ph.D. degree with the Department of Cognitive Communications.

He was a visiting Ph.D. student with the University of Leeds from 2019 to 2020. His current research interests include machine learning with a focus on shallow neural networks applications, signal processing for broadband wireless communication systems, multiple antenna techniques, and wireless channel modeling.



Kai Mei received the master's degree from the National University of Defense Technology, in 2017, where he is currently pursuing the Ph.D. degree. His research interests include synchronization and channel estimation in OFDM systems and MIMO-OFDM systems, and machine learning applications in wireless communications.



Jibo Wei (Member, IEEE) received the B.S. and M.S. degrees from the National University of Defense Technology (NUDT), Changsha, China, in 1989 and 1992, respectively, and the Ph.D. degree from Southeast University, Nanjing, China, in 1998, all in electronic engineering. He is currently the Director and a Professor of the Department of Communication Engineering, NUDT. His research interests include wireless network protocol and signal processing in communications, more specially, the areas of MIMO, multicarrier transmission, cooperative communication, and cognitive network. He is a member of the IEEE Communication Society and also a member of the IEEE VTS. He also works as one of the editors of the Journal on Communications and is a Senior Member of the China Institute of Communications and Electronics.



Xiaochen Zhang is currently a graduate student at College of Electronic Science and Engineering from National University of Defense Technology (NUDT), Changsha, China. He received the B.S. degree from NUDT in 2018. His research interests include resource allocation, multi-access edge computing, machine learning and channel modeling.



Des McLernon (Member, IEEE) received his B.Sc and MSc degrees from the Queen's University of Belfast, N. Ireland. After working on radar systems research with Ferranti Ltd in Edinburgh, Scotland, he then joined Imperial College, University of London, UK, where he took his PhD in signal processing. His research interests are broadly within the domain of signal processing for wireless communications in which field he has published around 340 journal and conference papers. Finally, in what spare time remains, he plays jazz piano in restaurants and bars and was recently runner-up in the 2018 "Leeds Pub Piano" competition.



Syed Ali Raza Zaidi (Senior Member, IEEE) is currently a University Academic Fellow (Assistant Professor) in the broad area of Communication and Sensing for RAS. He was awarded J. W. and F. W. Carter Prize, was also awarded with COST IC0902, EPSRC, DAAD and Royal Academy of Engineering grants. He has published more than 100 technical papers in various top-tier IEEE Journals and conferences. His research interests include design and implementation of communication protocols for wireless networking specifically in the area of M2M.



Dongtang Ma (SM'13) received the B.S. degree in applied physics and the M.S. and Ph.D. degrees in information and communication engineering from the National University of Defense Technology (NUDT), Changsha, China, in 1990, 1997, and 2004, respectively. From 2004 to 2009, he was an Associate Professor with the College of Electronic Science and Engineering, NUDT. Since 2009, he is a professor with the department of cognitive communication, School of Electronic Science and Engineering, NUDT. From Aug. 2012 to Feb. 2013, he was a visiting professor at University of Surrey, UK. His research interests include wireless communication and networks, physical layer security, intelligent communication and network. He has published more than 150 journal and conference papers. He is one of the Executive Directors of Hunan Electronic Institute. He served as the TPC member of PIMRC from 2012 to 2020.